Target Indexing in SAR Images Using Scattering Centers and the Hausdorff Distance*

June Ho Yi
Advanced Image Technology Group
Korea Institute of Science and Technology
P. O. Box 131, Cheongryang
Seoul 130-650, Korea
Email: yi@willow.kist.re.kr

Abstract

This paper is concerned with efficient and accurate indexing for target recognition in SAR images. We present a method that efficiently retrieves correct object hypotheses using the major axis of a pattern of scattering centers in SAR images and the Hausdorff distance measure. The features that we use are the locations of scattering centers in SAR returns. Experimental results show that indexing using major axis efficiently narrows down the number of candidate hypotheses and that the Hausdorff distance measure performs well in picking the correct hypothesis. These properties of the algorithm along with computational efficiency make our method more attractive for practical purposes than other existing methods for target indexing in SAR images.

1 Introduction

Automatic target recognition (ATR) from synthetic aperture radar (SAR) imagery is an important aspect of current vision research. Some of the representative work in ATR from SAR images includes [5] [8] and [12]. They focus on template matching techniques in which the templates are manually designed. However, few research works on target indexing using SAR images have been reported in the literature. Indexing is one of the fundamental issues in model-based recognition that is concerned with how to accurately and efficiently narrow down the number of candidate models to be matched without actually searching through all the models in a database. This research features accurate and efficient target indexing in SAR images given locations of scattering centers.

In indexing, the feature correspondence and search of model database are replaced by a table look-up mechanism. This indexing table is computed off-line. A brief survey of some representative object recognition systems that have employed geometric indexing or hashing techniques is given in Table 1. Performance of these systems cannot be compared directly because they have been developed based on different assumptions. They perform in different scenarios using different features to generate object hypotheses. More importantly, it is hard to compute complex structured features from point-like features that SAR returns although those approaches marked with asterisk (*) in Table 1 are potentially applicable to the problem of ATR from SAR images.

We have developed a computationally simple approach that efficiently retrieves correct model hypotheses when objects are represented by a pattern of point features. In the indexing table, model entries are indexed with the major axes of the patterns of scattering centers. We first index the input pattern of scattering centers using its major axis and validate candidate hypotheses using the Hausdorff distance measure. The Hausdorff distance is a method to determine the degree of resemblance between two objects when an object is represented by a set of point features. The method is quite tolerant of small positional errors. The Hausdorff distance will be described in section 3. Using the major axis indexing, candidate hypotheses whose major axes fall within some neighborhood of the major axis computed from the input pattern are quickly retrieved. The retrieved hypotheses are then rank-ordered in the increasing order of the Hausdorff distance measure and enter the verification stage in the order they are listed. Experimental results show that indexing using major axis is very efficient and that the Hausdorff distance measure performs very well in comparing positionally noisy patterns of scattering centers, resulting in accurate retrieval of the correct model hypothesis.

Let us briefly overview our entire target object recognition system. Figure 1 is a block diagram of the computation in the system. The entire system is divided into two parts: off-line simulation of SAR signatures of model objects and construction of indexing table and on-line recognition. In the off-line

*Part of this research was conducted while the author was with the Visualisation and Intelligent Systems laboratory, University of California, Riverside, CA.

Table 1: State-of-the-art techniques for indexing. Approaches using structured features are marked with *.

year	system	acquisition /recognition	input data	indexing key	comments w.r.t SAR
94	Yi and Chelberg [13]	3D/3D	range image	LSG (Local Surface Group)	*
94	Califano and Mohan [4]	2D/2D	2D drawing	seven dimensional global invariants	*
93	Rigoutsos and Hummel [9]	2D/2D	intensity image	coordinates of scene points computed in the coordinate system formed by an ordered pair of scene points	point set matching (no SAR)
93	Beis and Lowe [3]	2D/3D	range image	three angles and ratio of the interior edge lengths from four straight-line segment chain	*
92	Stein and Medioni [10]	2D/2D	intensity image	super segments with several different cardinalities for edges	*
92	Stein and Medioni [11]	3D/3D	range image	3D super segments with several different cardinalities for edges and splashes	*
92	Flynn and Jain [6]	3D/3D	range image	two invariant feature values computed from a triple of scene surface patches that are simultaneously visible	*
88	Lamdan et al. [7]	2D/2D	intensity image	coordinates of scene points in the affine-transformed coordinate system formed by an ordered triplet of three scene points	point set matching (no SAR)

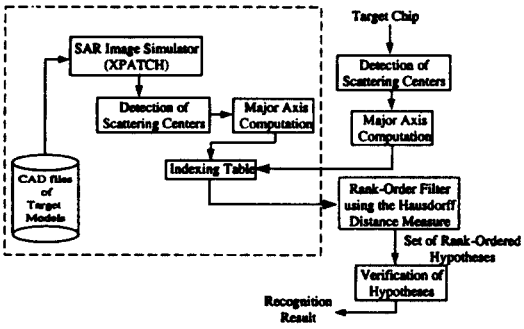

Figure 1: System Overview

part, SAR images of target models represented by CAD files are simulated with the XPATCH software [2] for a set of aspects (represented by *depression* and *azimuth* angles). For each image, locations of scattering centers are detected and its direction of major axis is computed. In the indexing table, model hypotheses represented by (*model name, depression angle, azimuth angle, location of scattering centers*) are linked to indexing keys that are directions of their major axes. At recognition time, scattering centers are extracted from the target chip. The major axis of the pattern of scattering centers is computed and models whose major axis is within $\pm\epsilon^\circ$ (threshold) neighborhood of the input major axis are quickly collected from the indexing table. At this stage, we apply the Hausdorff distance measure to match the scattering centers of the models and the target chip so as to validate the candidate hypotheses. We rank-order these hypotheses and they enter the verification stage in the order they are listed.

The contribution of this work is an efficient and accurate model retrieval method for target recognition in SAR images using a combination of the major axis analysis and the Hausdorff distance measure.

The following section presents the method to compute the major axis using the principal component analysis. Section 3 briefly describes the Hausdorff distance measure. Finally, section 4 reports experimental results for our current model database consisting of two armored vehicle targets, FRED and T72 tanks.

2 Computing Major Axis

We employed the principal component analysis to compute the major axis of a pattern of scattering centers. Principal component analysis is a well-known exploratory data analysis and is frequently used to reduce the data set's dimensionality and/or to extract new features from the original data which are uncorrelated. The use of this technique is specialised to two dimensions in this work, however, it can be used with input data of any dimensionality.

Assume that the input data is expressed as a matrix X with each row i containing the coordinates of one of the scattering centers $\mathbf{x}_i = (x_i, y_i)$:

$$\mathbf{X} = \begin{bmatrix} x_1 & y_1 \\ \vdots & \\ x_n & y_n \end{bmatrix}.$$

The following steps are performed using this input matrix:

1. The sample mean is computed for x and y coordinates as $\hat{\mu}_x = (1/n)\sum_{i=1}^{n} x_i$ and $\hat{\mu}_y = (1/n)\sum_{i=1}^{n} y_i$, respectively. A centered data ma-

trix $\mathbf{X}^*$ is constructed from $\mathbf{X}$:

$$\mathbf{X}^* = \begin{bmatrix} x_1 - \hat{\mu}_x & y_1 - \hat{\mu}_y \\ \vdots & \\ x_n - \hat{\mu}_x & y_n - \hat{\mu}_y \end{bmatrix}.$$

2. The sample covariance matrix $\hat{\mathbf{R}} = 1/n[\mathbf{X}^*]^t\mathbf{X}^*$ is obtained and its eigensystem is computed, yielding two eigenvalue and eigenvector pairs $\{(\mathbf{v}_1, \lambda_1), (\mathbf{v}_2, \lambda_2)\}$. Assume that the two pairs are sorted so that $\lambda_1 \geq \lambda_2$.

The two eigenvectors, $\mathbf{v}_1$ and $\mathbf{v}_2$, span the 2D imaging plane and the eigenvector $\mathbf{v}_1$ is the direction in the plane along which the data's sample variance is the larger (λ_1 is the sample variance along the direction). $\mathbf{v}_2$ is the direction orthogonal to $\mathbf{v}_1$ with the larger variance. The directionality of $\mathbf{v}_i$ is an excellent estimate of the orientation of scattering pattern. To resolve the 180° ambiguity, we use the direction that forms an acute angle with x axis as the direction of major axis.

3 The Hausdorff Distance Measure

Given two finite point sets $A = \{a_1, \cdots, a_p\}$ and $B = \{b_1, \cdots, b_q\}$, the Hausdorff distance is defined as

$$H(A, B) = \max(h(A, B), h(B, A)) \qquad (1)$$

where

$$h(A, B) = \max_{a \in A} \min_{b \in B} \|a - b\| \qquad (2)$$

and $\|\cdot\|$ is some underlying norm on the points of A and B.

Figure 2 illustrates the Hausdorff distance using two sets, A and B, consisting of two points. The function $h(A, B)$ is called the *directed* Hausdorff distance from A to B. It identifies the point $a \in A$ that is farthest from any point of B and measures distance from a to its nearest neighbor in B (using the given norm $\|\cdot\|$), that is, $h(A, B)$ in effect ranks each point of A based on its distance to the nearest point of B and then uses the largest ranked such point as the distance (the most mismatched point of A). Point of A must be within distance d of some points of B, and also there is some point of A that is exactly distance d from the nearest point of B (the most mismatched point). The Hausdorff distance $H(A, B)$ is the maximum of $h(A, B)$ and $h(B, A)$. Thus, it measures the degree of mismatch between two sets by measuring the distance of the point of A that is farthest point of any point of B and vice versa. The notion of resemblance encoded by this distance measure is that each member of A be near some member of B and vice versa. Unlike most methods of comparing shapes, there is no explicit pairing of points of A with points of B (for example, many points of A may be close to the same point of B). The function $H(A, B)$ can be

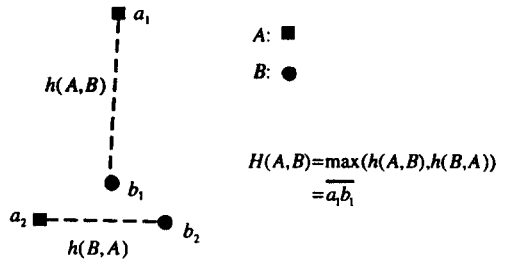

Figure 2: An illustration of the Hausdorff distance

trivially computed in time $O(pq)$ for two point sets of size p and q, respectively, and this can be improved to $O((p+q)\log(p+q))$ [1].

4 Experimental Results

The current model database includes two armored vehicle targets, FRED tank and T72 tank. The radar signature predictions (at six inch resolution for all azimuths from 0° to 359° in 1° steps at 15° elevation) of these tanks are generated using the XPATCH SAR simulation code.

We employ the following method to detect scattering centers. Other, more complicated, methods can be used, as long as they produce locations of scattering centers. We consider current pixel location a candidate scattering center if the magnitude of SAR return at the current pixel is a local maximum in the local neighborhood shown in Figure 3. Current pixel location is considered a local maximum if the following four conditions are met.

$$\begin{gathered} z(i,j-2)<z(i,j-1)<z(i,j)>z(i,j+1)>z(i,j+2) \\ \text{and} \\ z(i-2,j)<z(i-1,j)<z(i,j)>z(i+1,j)>z(i+2,j) \\ \text{and} \\ z(i-1,j-1)<z(i,j)>z(i+1,j+1) \\ \text{and} \\ z(i-1,j+1)<z(i,j)>z(i+1,j-1), \end{gathered} \qquad (3)$$

where $z(i, j)$ represents the magnitude of the image at the current pixel location, (i, j). The same method is used for detection of scattering centers at both off-line and on-line processes. Examples of scattering centers detected using this method and major axes computed from these scattering centers are shown in Figures 4 and 5 for FRED tank and T72 tank at azimuth angles, 18° and 60°, respectively. Top twenty scattering centers in terms of magnitude are selected in this experiment. If the number of scattering centers is less than twenty, all available scattering centers are used. After all scattering centers are identified, indexing table is built where a model entry, (*model name, depression angle, azimuth angle, locations of scattering centers*), is linked to a leaf node of binary tree that spans a small range (ϵ) of directions containing

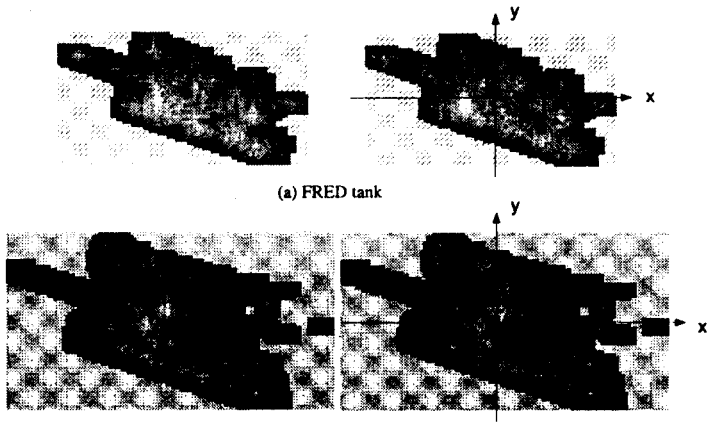

(a) FRED tank

(b) T72 tank

Figure 4: Magnitude of SAR returns (left) and scattering centers marked with small dark squares (right) for (a) FRED tank (b) T72 tank at azimuth angle 18° and elevation angle 15°. Only target region is taken from 256x256 target chip and zoomed in for clear visualization of scattering centers in the target. The original sizes of images in (a) and (b) are 85x45 and 111x60, respectively.

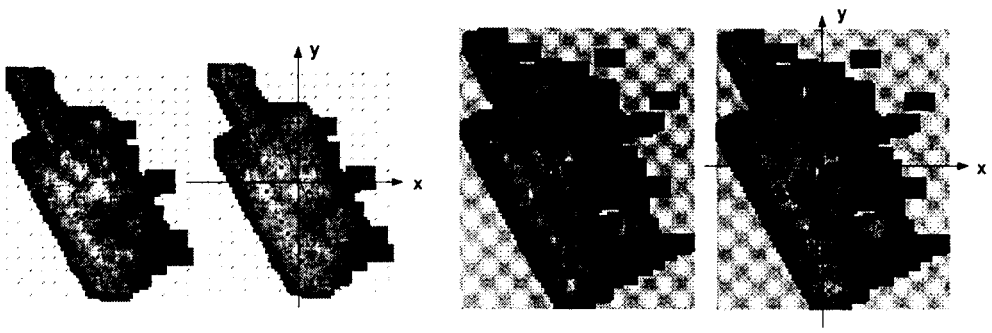

(a) FRED tank

(b) T72 tank

Figure 5: Magnitude of SAR returns (left) and scattering centers marked with small dark squares (right) for (a) FRED tank (b) T72 tank at azimuth angle 60° and elevation angle 15°. Only target region is taken from 256x256 target chip and zoomed in for clear visualization of scattering centers in the target. The original sizes of images in (a) and (b) are 62x78 and 78x93, respectively.

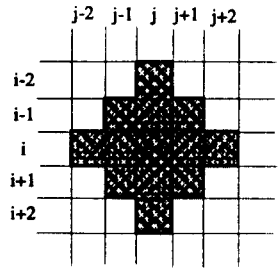

Figure 3: Local neighborhood (filled region) that is used to detect scattering centers

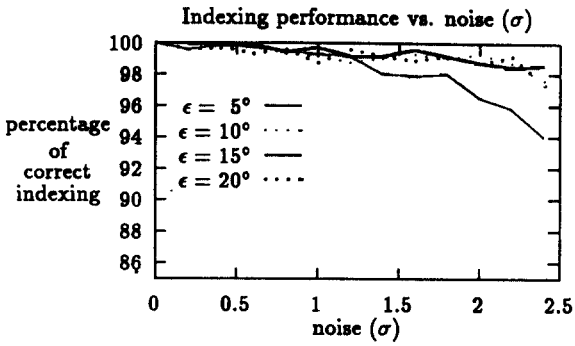

Figure 6: Indexing performance of the algorithm as the amount of positional noise varies: Indexing is considered successful when the first entry of the candidate list from the second Hausdorff stage is the correct answer. Models whose major axis is within ϵ° (threshold) neighborhood of the input major axis are quickly collected from the indexing table.

the major axis direction of the entry. Examples of these target signatures are shown in Figures 4 (left image) and 5 (left image).

For experiment, data for all azimuth angles from 0° to 359° are used as test data. We generate noisy locations of scattering centers, $(x + N_1(0,\sigma^2), y + N_2(0,\sigma^2))$, using two Gaussian random noise generators, N_1 and N_2. (x,y) is a noiseless location of a scattering center and $N(0,\sigma^2)$ denotes Gaussian noise of mean, 0, and standard deviation, σ. We have employed a rather strict requirement for a successful indexing. We consider an indexing result correct only when the first model entry ordered by the Hausdorff distance measure is the same as the input. Figure 6 shows the indexing performance of our method as the amount of positional noise added to location of scattering centers varies. Even though the amount of noise increases, the accuracy of indexing does not degrade significantly. As expected, the result shows that we need to use larger value of ϵ° to retrieve model hypotheses when noise gets large.

5 Conclusions

We have proposed an efficient method to retrieve object hypotheses using the major axis indexing and the Hausdorff distance measure. The major axis indexing technique efficiently narrows down the number of candidate hypotheses. The Hausdorff distance measure performs well in picking the correct hypothesis and is quite tolerant of positional errors in locations of scattering centers. These properties of the algorithm along with computational efficiency make the proposed method practically more attractive than other existing methods for target indexing in SAR images.

Acknowledgements

The synthetic SAR data used in this work were generated by Grinnell Jones in the Visualization and Intelligent Systems laboratory, University of California, Riverside.

References

[1] E. Alt, B. Behrends, and J. Blomer. Measuring the resemblance of polygonal shapes. In *Proceedings of the Seventh ACM Symposium on Computational Geometry*, 1991.

[2] D. J. Andersh, S. W. Lee, H. Ling, and C. L. Yu. Xpatch: A high frequency electromagnetic scattering prediction code using shooting and bouncing ray. In *Proceedings of Ground Target Modeling and Validation Conference*, pages 498–507, August 1994.

[3] Jeffrey Beis and David Lowe. Learning indexing functions for 3-D model-based object recognition. In *AAAI Workshop*, April 1993.

[4] Andrea Califano and Rakesh Mohan. Multidimensional indexing for recognizing visual shapes. *IEEE Transactions on Pattern Analysis and Machine Intelligence*, April 1994.

[5] D. E. Dudgeon, R. J. Lacoss, C. H. Lazott, and J. G. Verly. Use of persistent scatterers for model-based recognition. In *SPIE*, volume 2230, pages 356–368, Orlando, FL, April 1994.

[6] P. Flynn and A. K. Jain. Object recognition using invariant feature indexing of interpretation tables. *CVGIP: Image Understanding*, March 1992.

[7] Y. Lamina, J. Schwartz, and H. Wolfson. Object recognition by affine invariant matching. In *Proc. IEEE Conf. on Computer Vision and Pattern Recognition*, June 1988.

[8] L. M. Novak, G. J. Owirka, and C. M. Netishen. Performance of a hight-resolution polarimetric sar automatic target recognition system. *The Lincoln Laboratory Journal*, 6(1):11–24, 1993.

[9] I. Rigoutsos and R. Hummel. Distributed Bayesian object recognition. In *Proc. IEEE Conf. on Computer Vision and Pattern Recognition*, June 1993.

[10] F. Stein and G. Medioni. Structural indexing: Efficient 2-D object recognition. *IEEE Transactions on Pattern Analysis and Machine Intelligence*, 14(12):1198–1204, December 1992.

[11] F. Stein and G. Medioni. Structural indexing: Efficient 3-D object recognition. *IEEE Transactions on Pattern Analysis and Machine Intelligence*, 14(2):125–145, February 1992.

[12] A. M. Waxman, M. Seibert, A. M. Bernardon, and D. A. Fay. Neural systems for automatic target learning and recognition. *The Lincoln Laboratory Journal*, 6(1):77–116, 1993.

[13] J. H. Yi and D. M. Chelberg. Rapid obeject recognition from a large model database. In *Proceedings of the 2nd IEEE CAD-Based Workshop*, 1994.